Acta Mech 228, 2455–2470 (2017)
DOI 10.1007/s00707-017-1824-5

ORIGINAL PAPER

Michael Baumgart · Andreas Steinboeck · Martin Saxinger · Andreas Kugi

Elasto-plastic bending of steel strip in a hot-dip galvanizing line

Received: 9 January 2016 / Revised: 5 February 2017 / Published online: 11 April 2017

Abstract A quasi-static model of axially moving steel strips in a continuous hot-dip galvanizing line is presented. The model provides the bending line of the strip and takes into account the history of elasto-plastic deformation. The numerical integration of the material model of elasto-plastic deformation is algorithmically separated from the solution of the boundary value problem of the bending line by pre-computing sets of one-dimensional candidate relations between the strip curvature and the bending moment. Using this model, the influence of different roll positions in the zinc bath on the mean displacement of the strip at the gas wiping dies and the maximum lateral curvature of the strip (crossbow) can be efficiently calculated and analyzed.

1 Introduction

In continuous hot-dip galvanizing lines, cf. Fig. 1, the strip—subject to tension and high temperatures—may be plastically bent at the deflection rollers of the plant. These repeating bending actions cause deviations of the strip from the ideal flat shape in form of a coil-set or a crossbow. Here, the terms coil-set and crossbow refer to curvatures of the strip in longitudinal and lateral direction, respectively.

Just above the zinc bath, the strip passes so-called gas wiping dies which remove excess zinc and in this way control the thickness and uniformity of the zinc coating. Because a crossbow can lead to an inhomogeneous coating, the correction roll and the stabilization roll should effectively reduce this shape defect by means of controlled plastic bending of the strip. Basically, the zinc bath rolls build up a three-roll tension leveler. The positions of the bottom roll and the stabilization roll are fixed. The correction roll can be adjusted in z-direction and therefore serves as the input to control the strip shape. After the gas wiping dies, the zinc solidifies before the strip is deflected again at the tower roll.

First results of this paper have been presented by the authors at the Mini-Symposium "Axially Moving Structures" at PCM-CMM-2015 Conference in Gdansk, see [1].

M. Baumgart (✉) · M. Saxinger · A. Kugi
Christian Doppler Laboratory for Model-Based Control in the Steel Industry, Automation and Control Institute, Vienna University of Technology, Gußhausstraße 27-29, 1040 Vienna, Austria
E-mail: baumgart@acin.tuwien.ac.at

M. Saxinger
E-mail: saxinger@acin.tuwien.ac.at

A. Kugi
E-mail: kugi@acin.tuwien.ac.at

A. Steinboeck
Automation and Control Institute, Vienna University of Technology, Gußhausstraße 27-29, 1040 Vienna, Austria
E-mail: andreas.steinboeck@tuwien.ac.at

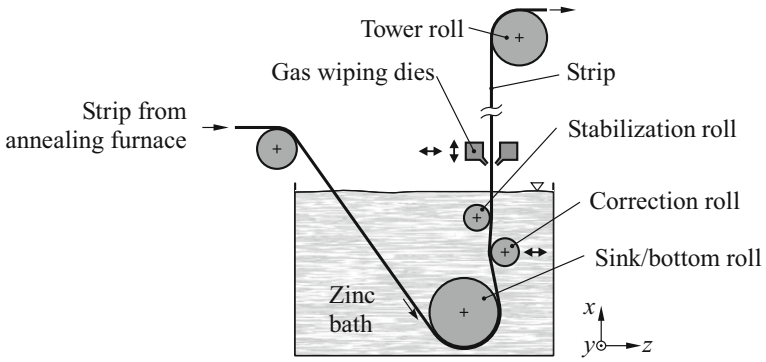

Fig. 1 Sketch of hot-dip galvanizing line

In order to optimally control the position of the correction roll and the gas wiping dies, a computationally efficient mathematical model of the shape in terms of the transversal deflection of the strip is required. A principal challenge of modeling the strip in the hot-dip galvanizing line is that the history of elasto-plastic deformation has to be considered. Effectively, a state variable that describes the elasto-plastic deformation history of each material point has to be conceptually moved with the strip through the plant. Furthermore, material models for plastic deformation are generally nonlinear and have to be numerically integrated along the deformation increments. Moreover, at the correction and the stabilization roll, the degree of deformation in terms of the strip curvature is a priori unknown. In [8], empirical relations for the strip curvatures at the correction and stabilization roll are used that were originally found for tension levelers [9]. Hira et al. [5] reported that these empirical relations are not accurate enough. A model of the strip in a tension leveler was proposed by Steinwender et al. [16,17]. However, the evolution and the transport of the intrinsic residual quantities due to plastic deformation still have to be computed along with the determination of the shape of the strip. Stadler et al. [14] presented a model for the special case of periodic elasto-plastic bending of a strip which is transported on rollers in a strip processing plant. Here only a uniaxial ideal-elastic ideal-plastic material is employed and the bending line is systematically solved for the a priori unknown contact points between the strip and the rolls. Generally, the problem can be solved by fully discretized FE models, which usually entail high computational costs [6,16].

In this paper, a first-principle, quasi-static model of the elasto-plastic bending line of the strip is presented. Because the model will be used for feedforward control and dynamic optimization of the adjustment of the gas wiping dies, emphasis is put on computational efficiency and low numerical complexity, thereby accepting a lower global accuracy. Thus, supposing small deformations, the one-dimensional model focuses on the transversal displacement in order to calculate the mean strip displacement at the gas wiping dies. Based on the results in [5,8], in the framework of small strain plasticity, the history of plastic deformation up to the stabilization roll is systematically taken into account assuming a plane state of stress. Thus, residual curvatures of the strip after the stabilization roll such as crossbow and coil-set can be calculated. Moreover, the numerical integration of the model of elasto-plastic deformation is algorithmically separated from the calculation of the actual bending line. This is facilitated by the following simplifications. Assuming Euler–Bernoulli hypotheses, the distribution of the longitudinal strain (in transport direction of the strip) over strip thickness is expressed in terms of the strip curvature and a mean longitudinal strain. Furthermore, the longitudinal tension force is assumed to be uniform in longitudinal direction and the mean strain is adapted in each deformation increment in order to meet this constraint. In fact, sets of candidate relations between the strip curvature and the bending moment are computed and stored in lookup tables (LUT) before the calculation of the bending line. From these sets, concurrent with the numerical solution of the bending line, those relations are determined that fulfill the balance equations of the problem. In this way, the influence of different roll settings on the strip displacement can be efficiently calculated and analyzed.

This paper is structured as follows: In Sect. 2, the detailed configuration of the strip and the rolls in the zinc bath is described and basic assumptions are introduced. In Sect. 3, the elasto-plastic material model based on the Prandtl–Reuß equations is summarized and customized for the application of strip bending in the hot-dip galvanizing line. The numerical implementation of this model, which relates the curvature and the bending moment of the strip, is briefly discussed. The differential equation for the displacement of the strip subject to tension and bending is derived in Sect. 4. The numerical discretization of the boundary value problem of the strip bending is presented and an algorithm to find the unknown points of contact between the strip and the

rolls is proposed. Results of simulation studies and a model validation based on measurements are shown in Sect. 5. Conclusions are given in Sect. 6.

2 Problem configuration and fundamental modeling assumptions

Figure 2 shows the rolls and the considered domain of the strip. Consider that the roll $\rho \in \{\mathrm{BR}, \mathrm{CR}, \mathrm{SR}, \mathrm{TR}\}$ has the center position x_ρ and the radius r_ρ. In the considered domain, the roll touches the strip at the a priori unknown points

$$x_\rho^{\mathrm{c}} = \begin{cases} x_\rho + r_\rho \sin(\alpha_\rho^{\mathrm{c}}) & \text{for } \rho \in \{\mathrm{BR}, \mathrm{SR}\}, \\ x_\rho - r_\rho \sin(\alpha_\rho^{\mathrm{c}}) & \text{for } \rho \in \{\mathrm{CR}, \mathrm{TR}\}, \end{cases} \tag{1}$$

where α_ρ^{c} refers to the angular position of these contact points. The z-coordinates w_ρ^{c} of these contact points read as

$$w_\rho^{\mathrm{c}} = \begin{cases} r_\rho \left(\cos(\alpha_\rho^{\mathrm{c}}) - 1\right) & \text{for } \rho \in \{\mathrm{BR}, \mathrm{SR}\}, \\ r_\rho \left(1 - \cos(\alpha_\rho^{\mathrm{c}})\right) - z_{\mathrm{CR}} & \text{for } \rho = \mathrm{CR}, \\ r_\rho \left(1 - \cos(\alpha_\rho^{\mathrm{c}})\right) & \text{for } \rho = \mathrm{TR}, \end{cases} \tag{2}$$

where $z_{\mathrm{CR}} > 0$ is the horizontal center displacement of the correction roll, which serves as a control input, see Fig. 2. Outside the considered domain, i.e., for $x < x_{\mathrm{BR}}^{\mathrm{c}}$ and $x > x_{\mathrm{TR}}^{\mathrm{c}}$, the strip wraps around the bottom roll and the tower roll, respectively. There, the strip is bent with the constant curvature $\kappa_\rho = r_\rho^{-1}$ defined by the radius r_ρ, $\rho \in \{\mathrm{BR}, \mathrm{TR}\}$, of the respective roll. Here, the thickness of the strip is small compared to the roll diameter and thus neglected.

In Sect. 4.1, the quasi-stationary boundary value problem (BVP) for the bending line of the strip in the domain $x_{\mathrm{BR}}^{\mathrm{c}} < x < x_{\mathrm{TR}}^{\mathrm{c}}$ is formulated. Replacing the empirical formulations used in [5,8], this allows to calculate the unknown peak curvatures at the correction roll and the stabilization roll based on first principles. Together with the deformation history defined by the bends at the bottom roll and at the deflection rolls of the upstream sections of the plant, these curvatures determine the state of elasto-plastic deformation of the strip after the stabilization roll.

Models developed in [16,17] describe the deformation of the strip along its complete path through a tension leveler, where the strip may usually wrap around the rolls, e.g., the bridle rolls. Clearly, this involves large deformation with considerable rotations. As pointed out in [16,17], consideration of these effects entails significant computational effort. For the considered hot-dip galvanizing line, the deformation is modeled in particular between the bottom and the tower roll, where under most operating conditions the strip does not wrap around the correction roll and the stabilization roll. In this considered domain, the highest deflection is determined by the adjustment z_{CR} of the correction roll relative to the ideal passline of the strip. For the considered plant (cf. Table 1), the maximum slope $\mathrm{d}w/\mathrm{d}x$ of the strip can be estimated by

$$-\frac{z_{\mathrm{CR}}}{x_{\mathrm{CR}} - x_{\mathrm{BR}}} \approx \frac{z_{\mathrm{CR}}}{x_{\mathrm{SR}} - x_{\mathrm{CR}}} \approx 0.15$$

for the majority of practical values $z_{\mathrm{CR}} \leq 60\,\mathrm{mm}$. Based on this observation, only small deformations of the strip and small contact angles ($|\alpha_\rho^{\mathrm{c}}| \ll 1$) are assumed. Furthermore, the Euler–Bernoulli hypothesis for beam bending is assumed. Consequently, based on the assumption of small angles, it is decisive for the accuracy of the model that

$$\left|\frac{\mathrm{d}w}{\mathrm{d}x}\right| < w'_{\max}, \quad x_{\mathrm{BR}}^{\mathrm{c}} < x < x_{\mathrm{TR}}^{\mathrm{c}}$$

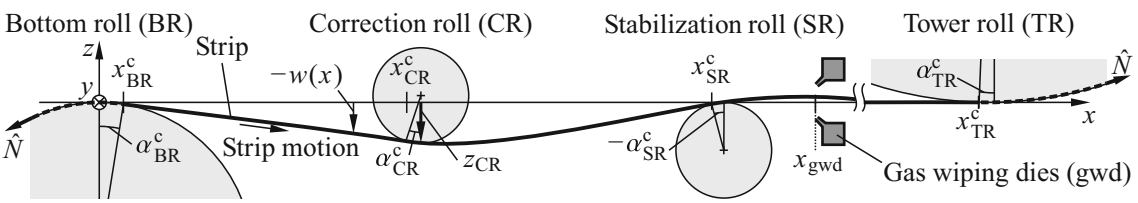

Fig. 2 Roll configuration

is met for the considered application. Generally, the parameter $w'_{\max}$ has to be determined by more accurate models of higher order, which is beyond the scope of this paper.

In longitudinal direction, a tension controller sets a constant strip tension at a driven roll just before the bottom roll and a speed controller sets the strip speed at the driven tower roll. Generally, the tension force in the strip increases between the bottom roll and the tower roll. The tension difference between these rolls carries the weight of the strip, drives the undriven zinc bath rolls, and performs the work of the plastic deformation. In this paper, the strip deflection w in the domain $x \leq x_{\mathrm{gwd}}$ is of particular interest. Because of $x_{\mathrm{gwd}} \ll x_{\mathrm{TR}}$, the gravitational force of the strip in this domain is small compared to the tension force $\hat{N}$ and thus is neglected for $x \leq x_{\mathrm{gwd}}$. In the domain $x > x_{\mathrm{gwd}}$, the strip is almost straight. Here, the tension force has only a minor influence on the quasi-static bending deformation of the strip. Thus, the gravitational force is also neglected in this domain. Moreover, friction forces at the pivot-mounted zinc bath rolls are neglected. Thus, the contact forces at the rolls have only radial components, meaning that together with the assumption of small contact angles $\alpha^{\mathrm{c}}_{\rho}$, the longitudinal component is negligibly small. In addition, also the change in tension due to plastic work is neglected. In the considered application, strip speeds are about $2\,\mathrm{ms}^{-1}$ and the total elongation of the strip between bottom roll and tower roll is small (maximum longitudinal plastic strain is about $4 \times 10^{-4}\,\mathrm{mm}^{-1}$ for the load cases considered in this paper). Thus, the increase in kinetic energy of the strip is small and the respective difference of the tensional force for accelerating the strip is neglected. Hence, the strip is assumed to be subject to a uniform tensional force $\hat{N}$. This central assumption decouples the transversal deflection from the momentum balance in longitudinal direction.

3 Material model of elasto-plastic strip bending

3.1 Stress–strain relations: Prandtl–Reuß equations

A common model describing the incremental elasto-plastic deformation are the Prandtl–Reuß equations, cf. [4,10,18] for the theoretical foundations and [8,9] for their application to strip processing lines. In the following, the Prandtl–Reuß equations are briefly repeated from the literature.

Generally, the Prandtl–Reuß equations are used in conjunction with the yield law of von Mises, which is known to give good results for metal plasticity [4]. Utilizing Einstein summation convention, von Mises' yield condition reads as

$$s_{ij}s_{ij} - \frac{2}{3}\sigma^2_{\mathrm{yld}} = 0, \tag{3}$$

where

$$s_{ij} = \sigma_{ij} - \frac{1}{3}\sigma_{kk}\delta_{ij} \tag{4}$$

are the components of the deviatoric stress tensor, σ_{ij} the components of the stress tensor, δ_{ij} is the Kronecker delta, and $i, j, k \in \{x, y, z\}$. The parameter σ_{yld} is the yield stress, a quantity referring to a uniaxial stress state which is usually obtained experimentally. Generally, σ_{yld} may depend on additional parameters like the temperature and some hardening mechanism. Experience from the plant operators indicates that for typical materials under usual operating conditions no distinct hardening mechanism is observed. Moreover, specific parameters for such mechanisms are not readily available. Hence, strain hardening is not considered and ideal-elastic ideal-plastic material behavior is subsequently used. In the zinc bath and in upstream process steps, the strip temperature exceeds 460 °C and thus the yield stress σ_{yld} is significantly lower than at room temperature. Because the strip temperature does not vary much while the strip travels through the zinc bath, σ_{yld} is assumed to be constant during this phase. Generally, thermal expansion is not considered.

For the hot-dip galvanizing line, the dependence of the yield stress on the deformation rate can be neglected because the deformation rates are low. For a material point, the Prandtl–Reuß equations describe the total strain increment $\mathrm{d}\varepsilon_{ij}$ and take the form [10]

$$\mathrm{d}\varepsilon_{ij} = \frac{1+\nu}{E}\mathrm{d}\sigma_{ij} - \frac{\nu}{E}\mathrm{d}\sigma_{kk}\delta_{ij} + \frac{3}{2}\frac{s_{ij}}{\sigma_{\mathrm{yld}}}\mathrm{d}\bar{\varepsilon}^{p}, \tag{5a}$$

where E is Young's modulus, ν is Poisson's ratio, and $\mathrm{d}\bar{\varepsilon}^{p}$ is the increment of the scalar-valued equivalent plastic strain.

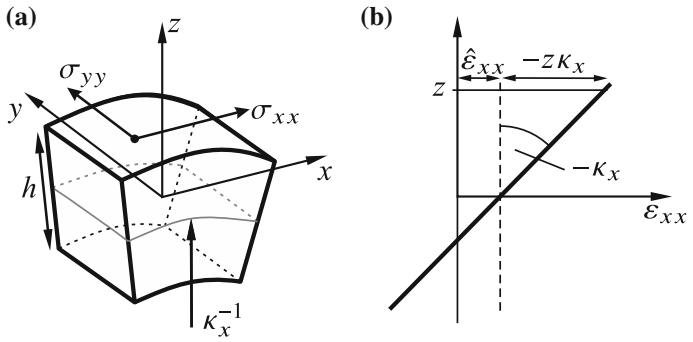

Fig. 3 **a** Infinitesimal strip element with plane state of stress and zero lateral curvature. **b** Relation between curvature and strain

For the elastic case, i.e., $s_{ij}s_{ij} < 2/3\sigma_{\text{yld}}^2$ and $\mathrm{d}\bar{\varepsilon}^p = 0$, (5a) exactly represents Hooke's law. In the elasto-plastic case, i.e., $\mathrm{d}\bar{\varepsilon}^p > 0$, the total derivative of the yield condition (3),

$$s_{ij}\mathrm{d}s_{ij} = 0, \tag{5b}$$

brings along an additional equation, which describes that the stresses remain on the yield surface during yielding. However, if hardening mechanisms should turn out to have significant influence, (5b) can be extended accordingly, see [18]. The set (5) consists of seven equations for the six components $\mathrm{d}\sigma_{ij}$ of the tensor of stress increments, the six components $\mathrm{d}\varepsilon_{ij}$ of the tensor of strain increments, and the increment of equivalent plastic strain $\mathrm{d}\bar{\varepsilon}^p$. In the next paragraphs, assumptions are made so that (5) can be uniquely solved for given strain increments in longitudinal direction of the strip, cf. [5,8,9].

The local coordinate system x–y–z used for the strip is shown in Fig. 3a. The longitudinal direction of the strip movement is the direction x. Because of the bending and tension loads, stress components in the x–y plane dominate compared to stress components in thickness direction. Hence, a plane state of stress and the Euler–Bernoulli hypothesis are assumed, i.e., $\sigma_{zz} = \sigma_{xz} = \sigma_{yz} = 0$. Because of this assumption, (5a) shows that also the shear strain increments $\mathrm{d}\varepsilon_{xz}$ and $\mathrm{d}\varepsilon_{yz}$ vanish. Moreover, it is assumed that the bending and tensional deformation is constant along the width direction y. Clearly, the rolls prevent a transversal deflection (along the direction z) and thus lateral curvature. Due to the Euler–Bernoulli hypothesis, this entails that the strain ε_{yy} is constant with respect to the thickness direction. Furthermore, the mean lateral contraction due to the longitudinal tension is assumed to be negligibly small. Hence, $\varepsilon_{yy} = 0$ ($\mathrm{d}\varepsilon_{yy} = 0$) is used. Strictly, this assumption entails nonvanishing stresses σ_{yy} in lateral direction at the strip edges, which cannot be carried by the rolls. However, as the strip is much wider than thick, this effect is assumed to be negligible in the sense of the principle of Saint-Venant. Moreover, vanishing (increments of) shear strains and stresses are assumed, i. e., $\mathrm{d}\varepsilon_{xy} = 0$, $\mathrm{d}\sigma_{xy} = 0$, $\varepsilon_{xy} = 0$, and $\sigma_{xy} = 0$, respectively. The change in the thickness is not of interest. Hence, $\mathrm{d}\varepsilon_{zz}$ is not considered in the following. Finally, the nonlinear relations between the longitudinal strain increment $\mathrm{d}\varepsilon_{xx}$ and the increment of equivalent plastic strain $\mathrm{d}\bar{\varepsilon}^p$ as well as the stress increments $\mathrm{d}\sigma_{xx}$ and $\mathrm{d}\sigma_{yy}$ can be found for the plastic domain in the form

$$\mathrm{d}\bar{\varepsilon}^p = \underbrace{\frac{2\,\sigma_{\text{yld}}\left(\nu\,\sigma_{xx} - 2\,\nu\,\sigma_{yy} - 2\,\sigma_{xx} + \sigma_{yy}\right)}{(4\,\nu - 5)\sigma_{xx}{}^2 + (8 - 10\,\nu)\sigma_{xx}\sigma_{yy} + (4\,\nu - 5)\sigma_{yy}^2}}_{e_p(\sigma_{xx},\sigma_{yy})}\mathrm{d}\varepsilon_{xx} \tag{6a}$$

$$\mathrm{d}\sigma_{xx} = \underbrace{-\frac{E\left(\sigma_{xx} - 2\,\sigma_{yy}\right)^2}{(4\,\nu - 5)\sigma_{xx}{}^2 + (8 - 10\,\nu)\sigma_{xx}\sigma_{yy} + (4\,\nu - 5)\sigma_{yy}^2}}_{g_{p,x}(\sigma_{xx},\sigma_{yy})}\mathrm{d}\varepsilon_{xx} \tag{6b}$$

$$\mathrm{d}\sigma_{yy} = \underbrace{-\frac{E\left(2\,\sigma_{xx} - \sigma_{yy}\right)\left(\sigma_{xx} - 2\,\sigma_{yy}\right)}{(4\,\nu - 5)\sigma_{xx}{}^2 + (8 - 10\,\nu)\sigma_{xx}\sigma_{yy} + (4\,\nu - 5)\sigma_{yy}^2}}_{g_{p,y}(\sigma_{xx},\sigma_{yy})}\mathrm{d}\varepsilon_{xx} \tag{6c}$$

For the elastic domain, the inequality

$$\sigma_{xx}^2 - \sigma_{xx}\sigma_{yy} + \sigma_{yy}^2 < \sigma_{\text{yld}}^2, \tag{7}$$

cf. (3), and

$$\mathrm{d}\bar{\varepsilon}^p = 0 \tag{8a}$$

hold. In this case, (5) (then representing Hooke's law) yields relations that are independent of the total stresses,

$$\mathrm{d}\sigma_{xx} = \frac{E}{1-\nu^2}\mathrm{d}\varepsilon_{xx} = g_{e,x}\mathrm{d}\varepsilon_{xx}, \tag{8b}$$

$$\mathrm{d}\sigma_{yy} = \frac{\nu E}{1-\nu^2}\mathrm{d}\varepsilon_{xx} = g_{e,y}\mathrm{d}\varepsilon_{xx}. \tag{8c}$$

Thus, at a given material point, the stresses and the state of plastic deformation only depend on the evolution of the longitudinal strain ε_{xx}. Starting from initial values $\sigma_{xx,0}$, $\sigma_{yy,0}$, and $\bar{\varepsilon}^p_0$, the absolute values can be obtained by integration of (6) or (8), e.g., for σ_{xx},

$$\sigma_{xx} = \int_{\varepsilon_{xx,0}}^{\varepsilon_{xx}} g_{\xi,x}(\sigma_{xx},\sigma_{yy})\mathrm{d}\tilde{\varepsilon}_{xx} + \sigma_{xx,0}, \tag{9}$$

where $\xi \in \{e, p\}$ depends on the yield condition (3).

3.2 Relation between bending moments and strip curvature

The stress resultants with respect to bending at a cross section of the strip with the height h and the width b are the bending moments

$$M_x = b\int_{-h/2}^{h/2} z\sigma_{xx}\mathrm{d}z, \tag{10a}$$

$$M_y = b\int_{-h/2}^{h/2} -z\sigma_{yy}\mathrm{d}z. \tag{10b}$$

Assuming small deformations and the Euler–Bernoulli hypothesis, the longitudinal strain ε_{xx} in (6)–(9) can be expressed in terms of the mean longitudinal strain $\hat{\varepsilon}_{xx}$ and the strip curvature κ_x, i. e.,

$$\varepsilon_{xx}(\hat{\varepsilon}_{xx},\kappa_x,z) = \hat{\varepsilon}_{xx} - z\kappa_x, \tag{11}$$

see Fig. 3b. The respective increment $\mathrm{d}\varepsilon_{xx}$ follows as

$$\mathrm{d}\varepsilon_{xx}(\hat{\varepsilon}_{xx},\kappa_x,z) = \mathrm{d}\hat{\varepsilon}_{xx} - z\mathrm{d}\kappa_x. \tag{12}$$

By inserting (9) into (10a), the bending moment M_x can be calculated for a given evolution of the strip curvature $\kappa_{x,0} \to \kappa_x$,

$$M_x = b\int_{-h/2}^{h/2} z\left(\int_{\varepsilon_{xx}(\hat{\varepsilon}_{xx,0},\kappa_{x,0},z)}^{\varepsilon_{xx}(\hat{\varepsilon}_{xx},\kappa_x,z)} g_{\xi,x}(\sigma_{xx},\sigma_{yy})\mathrm{d}\tilde{\varepsilon}_{xx}\right)\mathrm{d}z + \underbrace{b\int_{-h/2}^{h/2} z\sigma_{xx,0}\mathrm{d}z}_{=M_{x,0}}, \tag{13}$$

where $\hat{\varepsilon}_{xx,0}$, $\kappa_{x,0}$, and $M_{x,0}$ are the initial values of the mean longitudinal strain, the strip curvature, and the bending moment, respectively, at the beginning of the considered deformation.

The strip is subject to a tensional force $\hat{N}$, which is presumed to be uniform along the strip. Because the plastic bending of the cross section under tensional load leads to a permanent elongation of the strip, i.e., $\hat{\varepsilon}_{xx}$ increases, $\hat{\varepsilon}_{xx}$ in (11) is adjusted such that

$$\hat{N} = \underbrace{b\int_{-h/2}^{h/2}\left(\int_{\varepsilon_{xx}(\hat{\varepsilon}_{xx,0},\kappa_{x,0},z)}^{\varepsilon_{xx}(\hat{\varepsilon}_{xx},\kappa_x,z)} g_{\xi,x}(\sigma_{xx},\sigma_{yy})\mathrm{d}\tilde{\varepsilon}_{xx}\right)\mathrm{d}z}_{\stackrel{!}{=}0} + \underbrace{b\int_{-h/2}^{h/2}\sigma_{xx,0}\mathrm{d}z}_{=\hat{N}} \tag{14}$$

holds in each cross section of the strip, see [8]. Note that using (11) subject to (14) for the calculation of (9) leads to stress profiles that are asymmetric with respect to the mid-plane $z = 0$ of the strip.

As long as the deformation increment is purely elastic, the bending deformation does not alter the mean strain $\hat{\varepsilon}_{xx}$, i.e., $\mathrm{d}\hat{\varepsilon}_{xx} = 0$. The strain increments in (13) can then be written in terms of the strip curvature κ_x only, i.e., $\mathrm{d}\varepsilon_{xx} = -z\mathrm{d}\kappa_x$. By using (8) in (9), the linear elastic bending moment thus follows from (13) as

$$M_x = -K_b(\kappa_x - \kappa_{x,0}) + M_{x,0}, \tag{15}$$

where $K_b = Ebh^3/12(1-\nu^2)$ is the bending stiffness. For both the purely elastic and the elasto-plastic case, (13) constitutes a unique function $M_x(\kappa_x)$, as long as the deformation in terms of κ_x is monotonically increasing or decreasing.

3.3 Numerical implementation

For the computation of local stresses according to (9) and the stress resultants (10), the cross section is discretized along the direction z with the constant grid size Δz. Moreover, each interval of a monotonic deformation evolution $\kappa_{x,0} \to \kappa_x$ is equally discretized with the step size $\Delta\kappa_x$. At each spatial grid point z_i, the actual, finite strain increment follows from (12). Here, $\mathrm{d}\hat{\varepsilon}_{xx}$ is iteratively adjusted such that (14) holds for each step of κ_x.

If the deformation is elastic, (9) can be analytically solved. If at a spatial grid point z_i the current strain increment $\Delta\varepsilon_{xx}$ would cause the stresses to exceed the yield surface, i.e., $\sigma_{xx}^2 - \sigma_{xx}\sigma_{yy} + \sigma_{yy}^2 > \sigma_{\mathrm{yld}}^2$, the strain increment is divided into an elastic increment $\Delta\varepsilon_{xx}^e$ and an elasto-plastic increment $\Delta\varepsilon_{xx}^p$, i.e., $\Delta\varepsilon_{xx} = \Delta\varepsilon_{xx}^e + \Delta\varepsilon_{xx}^p$. The magnitude $\Delta\varepsilon_{xx}^e$ of the entirely elastic deformation step can be exactly calculated by inserting (9) with the expressions from (8) into the yield condition, cf. Eq. (7),

$$\sigma_{\mathrm{yld}}^2 = \left(-\frac{\Delta\varepsilon_{xx}^e E}{\nu^2-1} + \sigma_{xx,0}\right)^2 - \left(-\frac{\Delta\varepsilon_{xx}^e E}{\nu^2-1} + \sigma_{xx,0}\right)\left(-\frac{\nu\,\Delta\varepsilon_{xx}^e E}{\nu^2-1} + \sigma_{yy,0}\right) + \left(-\frac{\nu\,\Delta\varepsilon_{xx}^e E}{\nu^2-1} + \sigma_{yy,0}\right)^2. \tag{16}$$

From the two roots $\Delta\varepsilon_{xx,1}^e$ and $\Delta\varepsilon_{xx,2}^e$ of (16),

$$\Delta\varepsilon_{xx,1,2}^e = \frac{1}{2}\frac{\nu^2-1}{E(\nu^2-\nu+1)}\Big((2-\nu)\sigma_{xx,0} + (2\nu-1)\sigma_{yy,0} \pm \left(4(\nu^2-\nu+1)\sigma_{\mathrm{yld}}^2 - 3\nu^2\sigma_{xx,0}^2 + 6\nu\sigma_{xx,0}\sigma_{yy,0} - 3\sigma_{yy,0}^2\right)^{\frac{1}{2}}\Big), \tag{17}$$

the one is chosen whose sign corresponds to the current loading direction. In the elasto-plastic domain, (6) is integrated by means of the forward Euler method. If for the given strain increment (6a) would yield $\mathrm{d}\bar{\varepsilon}^p < 0$, the material point is elastically unloaded according to (8), starting from a stress state on the yield surface.

The numerical computation of the stresses can be considerably accelerated if the mean tensile stress due to the tensional force $\hat{N}$ is significantly smaller than σ_{yld}. In this case, the mean strain $\hat{\varepsilon}_{xx}$ in (11) and the constraint (14) can be neglected, i.e., pure bending is assumed. Hence, the stress increments at each spatial grid point z_i can be independently integrated, and due to symmetry, only one half of the strip thickness needs to be computed. A uniform discretization of the given deformation evolution $\kappa_{x,0} \to \kappa_x$ is not required. For each grid point, the complete step of elastic deformation can be determined by (17) and integrated in one step. For the elasto-plastic domain, the relations (6) are integrated by means of Runge–Kutta schemes with variable step length.

Finally, the stress resultants (10) are numerically integrated utilizing the trapezoidal rule at each point of the curvature grid. In Sect. 4.2, it will be motivated that in the considered application, the evolution of the deformation $\kappa_{x,0} \to \kappa_x$ is monotonic between two points of contact of the strip and the rolls. This monotonicity facilitates the use of unique one-dimensional lookup tables of the form $M_x(\kappa_x)$ and $M_y(\kappa_x)$. These lookup tables depend on the initial values of $\hat{\varepsilon}_{xx,0}$ and $\kappa_{x,0}$, and the initial profiles of $\sigma_{xx,0}(z)$, $\sigma_{yy,0}(z)$, and $\bar{\varepsilon}_0^p(z)$.

4 Quasi-static model of a strip under tension

4.1 Boundary value problem

The balance of forces and moments at an infinitesimal strip element, cf. Fig. 4, for $\mathrm{d}x \to 0$ reads as [2,3]

$$Q_x'(x) + q(x) = 0, \tag{18a}$$
$$M_x'(x) - Q_x(x) + \hat{N} w'(x) = 0, \tag{18b}$$

where the spatial derivative is denoted as $(\,\cdot\,)' = \mathrm{d}(\,\cdot\,)/\mathrm{d}x$. Due to the assumptions of small deformations, the forces in Fig. 4 are given with respect to the undeformed element. Distributed transversal loads, e. g., those caused by cooling air jets [13], are summarized in the load term $q(x)$. Differentiating (18b) with respect to x and inserting (18a) yields the differential equation for the quasi-static displacement $w(x)$ in z-direction [3,12,15],

$$M_x''(x) + \hat{N} w''(x) + q(x) = 0, \quad x \in (x^{\mathrm{c}}_{\mathrm{BR}}, x^{\mathrm{c}}_{\mathrm{TR}}) \backslash \{x^{\mathrm{c}}_{\mathrm{CR}}, x^{\mathrm{c}}_{\mathrm{SR}}\}. \tag{19}$$

Due to the elasto-plastic deformation, the bending moment $M_x(x)$ nonlinearly depends on the strip curvature $\kappa(x) \approx w''(x)$, cf. Sect. 3.

The BVP (19) is complemented by the following boundary and interface conditions at the contact points x^{c}_ρ with $\rho \in \{\mathrm{BR}, \mathrm{CR}, \mathrm{SR}, \mathrm{TR}\}$: At all contact points x^{c}_ρ, the deflection is prescribed by the roll surface as formulated in (2). Clearly, the strip touches the rolls tangentially. Hence, for small angles, the unknown contact angles α^{c}_ρ in (1) and (2) have to satisfy $w'(x^{\mathrm{c}}_\rho) = -\alpha^{\mathrm{c}}_\rho$. At $x^{\mathrm{c}}_{\mathrm{BR}}$, the curvature is given by the roll curvature, $w''(x^{\mathrm{c}}_{\mathrm{BR}}) = -r^{-1}_{\mathrm{BR}}$. The bending moment $M_{x,\mathrm{BR}}$ follows from the deformation history defined by the bends at upstream deflection rolls including the bottom roll. Hence, for the bottom roll

$$w(x^{\mathrm{c}}_{\mathrm{BR}}) = w^{\mathrm{c}}_{\mathrm{BR}}, \tag{20a}$$
$$w'(x^{\mathrm{c}}_{\mathrm{BR}}) = -\alpha^{\mathrm{c}}_{\mathrm{BR}}, \tag{20b}$$
$$M_x(x^{\mathrm{c}}_{\mathrm{BR}}) = M_{x,\mathrm{BR}} \quad \leftrightarrow \quad w''(x^{\mathrm{c}}_{\mathrm{BR}}) = -r^{-1}_{\mathrm{BR}} \tag{20c}$$

hold. At the intermediate rolls, i. e., $x = x^{\mathrm{c}}_\rho$, $\rho \in \{\mathrm{CR}, \mathrm{SR}\}$, the slope and the bending moment (and with it the curvature) have to be continuous:

$$w(x^{\mathrm{c}-}_\rho) = w(x^{\mathrm{c}+}_\rho) = w^{\mathrm{c}}_\rho, \tag{21a}$$
$$w'(x^{\mathrm{c}-}_\rho) = w'(x^{\mathrm{c}+}_\rho) = -\alpha^{\mathrm{c}}_\rho, \tag{21b}$$
$$M_x(x^{\mathrm{c}-}_\rho) = M_x(x^{\mathrm{c}+}_\rho) \quad \leftrightarrow \quad w''(x^{\mathrm{c}-}_\rho) = w''(x^{\mathrm{c}+}_\rho). \tag{21c}$$

Here, $x^{\mathrm{c}+}_\rho$ and $x^{\mathrm{c}-}_\rho$ indicate the right- and the left-hand side limit at the respective position. The boundary conditions at the tower roll are expected to have only minor influence on the strip displacement near the zinc bath rolls because the tower roll is far away from the stabilization roll. In fact, $x_{\mathrm{TR}} - x_{\mathrm{SR}} > 50\,\mathrm{m}$ holds. Hence,

$$x^{\mathrm{c}}_{\mathrm{TR}} = x_{\mathrm{TR}},$$
$$w(x^{\mathrm{c}}_{\mathrm{TR}}) = 0, \tag{22a}$$
$$w'(x^{\mathrm{c}}_{\mathrm{TR}}) = 0 \tag{22b}$$

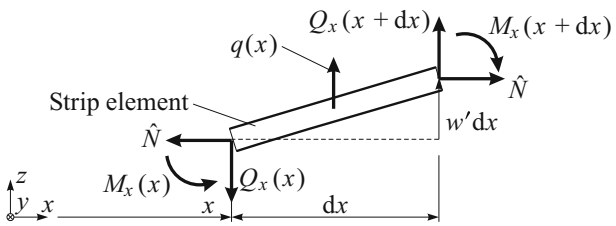

Fig. 4 Infinitesimal strip element with forces and moments

can be used. With (20), (21) for $\rho \in \{\mathrm{CR}, \mathrm{SR}\}$ and (22), 15 equations are defined for the determination of the 12 integration constants of the fourth-order BVP (19) in the three domains $x^{\mathrm{c}}_{\mathrm{BR}} < x < x^{\mathrm{c}}_{\mathrm{CR}}$, $x^{\mathrm{c}}_{\mathrm{CR}} < x < x^{\mathrm{c}}_{\mathrm{SR}}$, and $x^{\mathrm{c}}_{\mathrm{SR}} < x < x^{\mathrm{c}}_{\mathrm{TR}}$ and the three unknown contact points in terms of the contact angles $\alpha^{\mathrm{c}}_{\mathrm{BR}}$, $\alpha^{\mathrm{c}}_{\mathrm{CR}}$, and $\alpha^{\mathrm{c}}_{\mathrm{SR}}$.

Generally, the whole problem (19) with the boundary conditions (20)–(22) can be solved by means of some discretization scheme. However, the discretization of the large domain $x^{\mathrm{c}}_{\mathrm{SR}} < x < x^{\mathrm{c}}_{\mathrm{TR}}$ highly increases the dimension of the problem, although only the deflection of the strip close to the stabilization roll is of interest. Therefore, the problem is simplified by assuming elastic behavior, i.e., $\mathrm{d}\bar{\epsilon}^{p} = 0$, in the domain $x^{\mathrm{c}}_{\mathrm{SR}} < x < x^{\mathrm{c}}_{\mathrm{TR}}$, which holds true for most relevant operating conditions. In this case, and for vanishing $q(x)$, the affine constitutive law (15) holds and (19) has the analytical solution

$$w(x) = w_{\mathrm{SR|TR}}(x) = \underbrace{C_0 + C_1 x}_{\text{String solution}} + \underbrace{C_2 \exp\left(\left(\frac{\hat{N}}{K_b}\right)^{\frac{1}{2}} x\right) + C_3 \exp\left(-\left(\frac{\hat{N}}{K_b}\right)^{\frac{1}{2}} x\right)}_{\text{Bending solution}} \tag{23}$$

between the two points of contact $x^{\mathrm{c}}_{\mathrm{SR}}$ and $x^{\mathrm{c}}_{\mathrm{TR}}$, indicated by the subscript "SR|TR." This analytical solution consists of a linear part, the so-called string or membrane solution, and an exponential part, which describes the bending deformation. The boundary conditions (21a) and (21c) for $\rho = \mathrm{SR}$, and (22) are used to analytically determine the coefficients C_0 to C_3. The solution is thus parameterized by the a priori unknown value $w''(x^{\mathrm{c}}_{\mathrm{SR}}) = \kappa_{x,\mathrm{SR}}$, i.e., $w_{\mathrm{SR|TR}} = w_{\mathrm{SR|TR}}(x; \kappa_{x,\mathrm{SR}})$. The spatial derivative of this analytical expression at $x = x^{\mathrm{c}}_{\mathrm{SR}}$ replaces the continuity condition (21b) and the new boundary conditions at the stabilization roll read as

$$w(x^{\mathrm{c}}_{\rho}) = w^{\mathrm{c}}_{\rho}, \tag{24a}$$

$$w'(x^{\mathrm{c}}_{\mathrm{SR}}) = w'_{\mathrm{SR|TR}}(x^{\mathrm{c}}_{\mathrm{SR}}; \kappa_{x,\mathrm{SR}}) = -\alpha^{\mathrm{c}}_{\mathrm{SR}}. \tag{24b}$$

Hence, the bending line does not need to be solved numerically after the stabilization roll. The influence of this segment on the solution before the stabilization roll is now completely contained in the boundary condition (24b).

The assumptions that justify to model the strip as a one-dimensional beam do not strictly hold for $x > x^{\mathrm{c}}_{\mathrm{SR}}$, see also Sect. 4.5. Away from the rolls, the lateral bending moment M_y vanishes and the strip develops a deflection profile in lateral direction. However, comparisons with a plate model show that the solutions of these two models (in terms of the mean transverse deflection) agree very well, in particular in the domain of interest near the gas wiping dies. Hence, it can be concluded that the beam model is sufficiently accurate to compute the deflection of the strip at the gas wiping dies as well as the strip curvature w'' and the bending moment M_x in the region $x > x^{\mathrm{c}}_{\mathrm{SR}}$.

4.2 Deformation history of the quasi-static strip model

In transient operation situations, each cross section has its individual state and history of deformation, which is transported along with the strip. Considering this transport in numerical models involves significant computational effort, cf. [6]. However, in the considered quasi-static case, the bending line does not vary and each cross section undergoes the same evolution of curvature. Hence, only the deformation history of one example cross section needs to be considered to parametrize the constitutive law $M_x(\kappa_x)$ used in (19).

At $x^{\mathrm{c}}_{\mathrm{BR}}$, the initial profiles $\sigma_{xx,\mathrm{BR}}(z)$, $\sigma_{yy,\mathrm{BR}}(z)$, and $\bar{\varepsilon}^{p}_{\mathrm{BR}}(z)$ and the initial values $\hat{\varepsilon}_{xx,\mathrm{BR}}$, $\kappa_{x,\mathrm{BR}} = -r^{-1}_{\mathrm{BR}}$, and $M_{x,\mathrm{BR}}$ are defined by the deformation history in upstream process steps and at the bottom roll. In general, the direction of deformation in terms of the curvature κ_x between two rolls is not determined in advance but depends on the actual boundary conditions and the transverse loads, cf., e.g., [14]. However, as it turned out in all numerical investigations of the considered problem, under normal process conditions, vanishing transversal forces q and excluding strain-softening materials, the direction of the deformation is monotonic between the zinc bath rolls and changes only at the contact points x^{c}_{ρ}. Therefore, the constitutive relation (13) can be uniquely parameterized based on the deformation state at the closest upstream zinc bath rolls. Hence, the bending moment $M_x(x)$ can be formulated for the complete domain in the form

$$x^{\mathrm{c}}_{\mathrm{BR}} < x \leq x^{\mathrm{c}}_{\mathrm{CR}}: \; M_x(x) = M_{x,\mathrm{BR|CR}}(\kappa_x(x)), \tag{25a}$$

$$x^{\mathrm{c}}_{\mathrm{CR}} < x \leq x^{\mathrm{c}}_{\mathrm{SR}}: \; M_x(x) = M_{x,\mathrm{CR|SR}}(\kappa_x(x); \kappa_{x,\mathrm{CR}}), \tag{25b}$$

$$x^{\mathrm{c}}_{\mathrm{SR}} < x \leq x^{\mathrm{c}}_{\mathrm{TR}}: \; M_x(x) = M_{x,\mathrm{SR|TR}}(\kappa_x(x); [\kappa_{x,\mathrm{CR}}, \kappa_{x,\mathrm{SR}}]). \tag{25c}$$

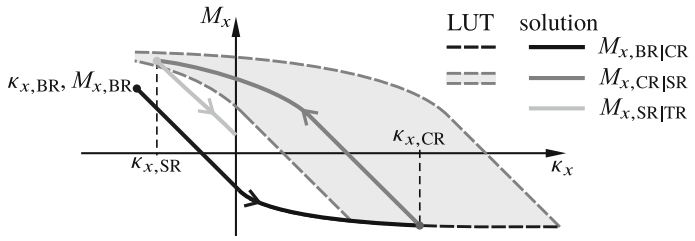

Fig. 5 Constitutive relation between the bending moment M_x and the strip curvature κ_x depending on the deformation history

Note that the right-hand sides of (25) depend also on $\hat{N}$, $\sigma_{xx,\mathrm{BR}}(z)$, $\sigma_{yy,\mathrm{BR}}(z)$, $\bar{\varepsilon}^p_{\mathrm{BR}}(z)$, $\hat{\varepsilon}_{xx,\mathrm{BR}}$, $\kappa_{x,\mathrm{BR}}$, and $M_{x,\mathrm{BR}}$. Because the deformation is assumed to be purely elastic in the domain $x^{\mathrm{c}}_{\mathrm{SR}} < x \le x^{\mathrm{c}}_{\mathrm{TR}}$, $M_{x,\mathrm{SR|TR}}$ can be analytically calculated, i.e.,

$$M_{x,\mathrm{SR|TR}} = -K_b(\kappa_x - \kappa_{x,\mathrm{SR}}) + M_{x,\mathrm{CR|SR}}(\kappa_{x,\mathrm{SR}}; \kappa_{x,\mathrm{CR}}). \tag{26}$$

The relations $M_{x,\mathrm{BR|CR}}(\kappa_x)$ and $M_{x,\mathrm{CR|SR}}(\kappa_x; \kappa_{x,\mathrm{CR}})$ are numerically computed as described in Sect. 3.3 for a set of different candidate curvatures $\kappa_{x,\mathrm{CR}}$, and the results are stored in a one- and a two-dimensional LUT, respectively, before solving the BVP (19). In this way, the constitutive relations (25) can be reused when the BVP is solved for different roll settings. Figure 5 shows examples of these relations as piecewise defined functions. The actual curvatures $\kappa_{x,\mathrm{CR}}$ and $\kappa_{x,\mathrm{SR}}$ are finally obtained together with the solution of the BVP (19) with the boundary conditions (20), (21) for $\rho = \mathrm{CR}$, (24), and subject to (25).

4.3 Numerical implementation

The nonlinear BVP (19) is discretized by means of finite elements. For the finite element shown in Fig. 6, the weak form of (19) corresponds to the virtual work δW of the forces and moments, which can be written in the form

$$\begin{aligned}\delta W = 0 = \int_{x_1}^{x_2} \left(-M_x \delta w'' + \hat{N} w' \delta w' - q \delta w\right) \mathrm{d}x \\ - Q_1 \delta w(x_1) - Q_2 \delta w(x_2) + M_1 \delta w'(x_1) + M_2 \delta w'(x_2),\end{aligned} \tag{27}$$

cf. [2,11]. The deflection, the slope, and the curvature at the element nodes are chosen as the degrees of freedom, i.e.,

$$\boldsymbol{u} = \left[w(x_1), w'(x_1), w''(x_1), w(x_2), w'(x_2), w''(x_2)\right]^{\mathsf{T}}. \tag{28}$$

This choice ensures continuity of w, w', and w'' at the element interfaces.

For each element of length $\Delta x = x_2 - x_1$, the Galerkin weighted residual method is used with trial functions in the form of Hermite polynomials of fifth order. This gives

$$w(x) = \begin{bmatrix} 1 - 10\frac{(x-x_1)^3}{\Delta x^3} + 15\frac{(x-x_1)^4}{\Delta x^4} - 6\frac{(x-x_1)^5}{\Delta x^5} \\ (x-x_1)\left(1 - 6\frac{(x-x_1)^2}{\Delta x^2} + 8\frac{(x-x_1)^3}{\Delta x^3} - 3\frac{(x-x_1)^4}{\Delta x^4}\right) \\ \frac{(x-x_1)^2}{2}\left(1 - 3\frac{x-x_1}{\Delta x} + 3\frac{(x-x_1)^2}{\Delta x^2} - \frac{(x-x_1)^3}{\Delta x^3}\right) \\ 10\frac{(x-x_1)^3}{\Delta x^3} - 15\frac{(x-x_1)^4}{\Delta x^4} + 6\frac{(x-x_1)^5}{\Delta x^5} \\ -(x-x_1)\left(4\frac{(x-x_1)^2}{\Delta x^2} - 7\frac{(x-x_1)^3}{\Delta x^3} + 3\frac{(x-x_1)^4}{\Delta x^4}\right) \\ \frac{(x-x_1)^2}{2}\left(\frac{x-x_1}{\Delta x} - 2\frac{(x-x_1)^2}{\Delta x^2} + \frac{(x-x_1)^3}{\Delta x^3}\right) \end{bmatrix}^{\mathsf{T}} \boldsymbol{u} = \boldsymbol{H}^{\mathsf{T}}(x)\boldsymbol{u}, \quad x_1 < x \le x_2, \tag{29}$$

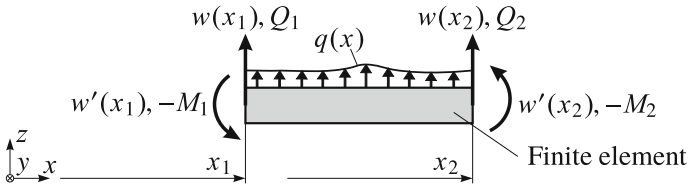

Fig. 6 Finite element with boundary forces and moments

cf. [11]. These fifth-order polynomials allow a quadratic approximation of the curvature inside each element. This takes into account that the curvature—due to the saturation characteristic of the elasto-plastic relation between the bending moment and the curvature—may change rapidly in regions where yielding occurs. Therefore, these tailored fifth-order polynomials generally reduce the required number of finite elements. By integration of (27) with $w(x)$ from (29), the nonlinear element function is obtained as

$$\hat{N}\mathbf{K}\boldsymbol{u} - \boldsymbol{f}_M(\boldsymbol{u}) = \left[Q_1, -M_1, 0, Q_2, -M_2, 0\right]^{\mathsf{T}} + \boldsymbol{f}_q(q). \tag{30}$$

The matrix

$$\mathbf{K} = \int_{x_1}^{x_2} \boldsymbol{H}'(x)\left(\boldsymbol{H}^{\mathsf{T}}\right)'(x)\,\mathrm{d}x \tag{31}$$

is constant. The integrand of

$$\boldsymbol{f}_M(\boldsymbol{u}) = \int_{x_1}^{x_2} M_x(\boldsymbol{H}''(x)\boldsymbol{u})\left(\boldsymbol{H}^{\mathsf{T}}\right)''(x)\,\mathrm{d}x \tag{32}$$

contains the nonlinear constitutive law (25). The load $\boldsymbol{f}_q$ enters the vector

$$\boldsymbol{f}_q(q) = \int_{x_1}^{x_2} q(x)\boldsymbol{H}^{\mathsf{T}}(x)\,\mathrm{d}x. \tag{33}$$

The integrals in (32) and (33) are computed by means of a fifth-order Gauss–Legendre quadrature. For assembling the complete set of equations in the considered domain $x^{\mathrm{c}}_{\mathrm{BR}} \le x \le x^{\mathrm{c}}_{\mathrm{SR}}$, the degrees of freedom at the element interfaces are set equal. At the point of contacts, the boundary and interface conditions (20a), (20c), (21a) for $\rho = \mathrm{CR}$, (24a), and (24b) define the respective nodal degrees of freedom and the bending moments. In Sect. 4.4, it is described how the remaining boundary and interface conditions are used to determine the contact angles α^{c}_ρ, $\rho \in \{\mathrm{BR}, \mathrm{CR}, \mathrm{SR}\}$.

The result (23) indicates for purely elastic sections that bending solutions exponentially decay away from the boundary points. Inspired by this observation, the step sizes of the FEM mesh are chosen as follows: Close to the rolls, a fine mesh is used which evolves from a minimum to a maximum step size according to a geometric series. In the region where the bending solution is expected to have decayed to a certain degree (e. g., to 1% of the initial value), the maximum step size is uniformly used. The algebraic problem (30) is assembled for all elements, normalized, and solved for $\boldsymbol{u}$ by means of the Newton–Raphson method. Here, a reasonable initial guess is found from the solution with purely elastic material behavior. Using this initial guess, the solution of the full elasto-plastic problem is obtained within 1–15 iterations depending on how much of the strip is plasticized.

4.4 Contact algorithm

Generally, the unknown contact angles α^{c}_ρ in (1) with $\rho \in \{\mathrm{BR}, \mathrm{CR}, \mathrm{SR}\}$ can be directly determined together with the solution of the FE equations (30) taking into account also the boundary conditions (20b), (21b) for $\rho = \mathrm{SR}$ and (24b). However, these conditions directly vary the domain boundaries x^{c}_ρ, cf. (1). A different approach for solving the contact problem is to introduce Lagrangian multipliers, cf., e.g., [16]. In this case, however, the applicable branch of the constitutive law (25) could change for elements that are candidates for being in contact with rolls because it is not clear in advance in which direction they are loaded. In order to avoid these kinds of problems, the contact conditions are solved in an outer loop by means of the fix-point iteration scheme

$$(\alpha^{\mathrm{c}}_\rho)_{i+1} = -w'\left(x^{\mathrm{c}}_\rho\left((\alpha^{\mathrm{c}}_\rho)_i\right)\right), \quad \rho \in \{\mathrm{BR}, \mathrm{CR}, \mathrm{SR}\} \tag{34}$$

with $x_\rho^{\mathrm{c}}((\alpha_\rho^{\mathrm{c}})_i)$ according to (1). In each iteration i, the nonlinear BVP (19) is solved in an inner loop with fixed boundaries. Usually, 2–5 iterations of (34) are required to solve the whole problem with sufficient accuracy.

Clearly, the radius of the strip curvature at the correction roll and the stabilization roll cannot exceed the respective roll radius. Hence, if the solution of the BVP (19) in an inner loop of the contact algorithm yields $w''(x_{\mathrm{CR}}^{\mathrm{c}}) \geq r_{\mathrm{CR}}^{-1}$, the problem is automatically reformulated and the bending line is solved only for the domain $x_{\mathrm{CR}}^{\mathrm{c}} \leq x \leq x_{\mathrm{TR}}^{\mathrm{c}}$. Because the curvature is now known at the correction roll, boundary conditions in analogy to (20) are defined at $x_{\mathrm{CR}}^{\mathrm{c}}$. The boundary conditions (24) at the stabilization roll remain the same and only the unknown contact angles $\alpha_{\mathrm{CR}}^{\mathrm{c}}$ and $\alpha_{\mathrm{SR}}^{\mathrm{c}}$ have to be determined. If the strip curvature reaches $w''(x_{\mathrm{SR}}^{\mathrm{c}}) = -r_{\mathrm{SR}}^{-1}$, a further increase in z_{CR} would not lead to a change in the crossbow deformation of the strip after the stabilization roll. In this case, the control input z_{CR} is saturated, which marks the limit of a meaningful operating range. Scenarios beyond this point do not need to be covered by the numerical analysis.

4.5 Maximum crossbow after the stabilization roll

Between the stabilization roll (SR) and the tower roll (TR), the strip passes a long segment without support (approximately 55 m). In this segment, the transversal deformation of the strip in lateral direction is not generally restricted. Here, the strip would be more accurately modeled as a plate rather than a beam, cf., e.g. [7], where the strip is modeled as a plate considering purely elastic deformation only. However, based on the state of elasto-plastic deformation calculated with the beam model and the material model (5) for plane stress, the tendency of the strip shape in lateral direction can be captured, cf. [5,8]. Far away from the rolls, the bending moment M_y, cf. (10b), of an ideal infinitely long strip must vanish as this long strip is essentially free in lateral direction. Because the elasto-plastic bending at upstream rolls also leads to a plastic deformation in lateral direction, the release of M_y gives rise to a lateral curvature (in width direction), the so-called crossbow.

Therefore, after the stabilization roll, the strain increment $\mathrm{d}\varepsilon_{yy}$ does not vanish and is thus related to the curvature κ_y, i.e., $\mathrm{d}\varepsilon_{yy} = -z\mathrm{d}\kappa_y$. Based on Hooke's law [i.e., (5) with $\mathrm{d}\bar{\varepsilon}^p = 0$], the relations

$$\mathrm{d}\sigma_{xx} = -z\frac{E}{1-\nu^2}(\mathrm{d}\kappa_x + \nu\mathrm{d}\kappa_y), \qquad \mathrm{d}\sigma_{yy} = -z\frac{\nu E}{1-\nu^2}(\nu\mathrm{d}\kappa_x + \mathrm{d}\kappa_y) \tag{35}$$

for the stress increments are obtained. The stabilization roll enforces $\kappa_{y,\mathrm{SR}} = 0$. By analogy to (13), inserting the integrals of (35) for given linear elastic deformations $\kappa_{x,\mathrm{SR}} \to \kappa_x$ and $0 \to \kappa_y$ into (10) yields

$$\begin{bmatrix} M_x \\ M_y \end{bmatrix} = K_b \begin{bmatrix} -1 & -\nu \\ \nu & 1 \end{bmatrix} \begin{bmatrix} \kappa_x - \kappa_{x,\mathrm{SR}} \\ \kappa_y \end{bmatrix} + \begin{bmatrix} M_{x,\mathrm{SR}} \\ M_{y,\mathrm{SR}} \end{bmatrix}. \tag{36}$$

Due to the straightening effect of the tensional force $\hat{N}$ on the large domain between stabilization roll and tower roll ($x_{\mathrm{SR}}^{\mathrm{c}} < x \leq x_{\mathrm{TR}}^{\mathrm{c}}$), it is assumed that the curvature κ_x is reduced to zero, $\kappa_x = 0$. The remaining curvature $\kappa_{y,\max}$ for entirely released bending moment $M_y = 0$ follows from (36) as

$$\kappa_{y,\max} = \nu\kappa_{x,\mathrm{SR}} - \frac{M_{y,\mathrm{SR}}}{K_b}. \tag{37}$$

With $\kappa_{y,\max}$ being constant along the strip width, the strip takes the form of a circular arc. The maximum deflection $\Delta w_{y,\max}$ of the strip (difference center-border) is thus approximated by

$$\Delta w_{y,\max} = -\frac{\kappa_{y,\max} b^2}{8}. \tag{38}$$

5 Numerical results

5.1 Simulation study

Typical parameters of a hot-dip galvanizing line and of an example strip are listed in Table 1. For these parameters, numerical results are presented that were computed with a MATLAB® implementation of the model on a standard PC (Quadcore CPU Intel i7 Haswell, 3.5 GHz, 16 GB RAM). With a reasonable discretization Δz of the strip thickness and $\Delta\kappa_x$ of the curvature evolution, cf. Table 1, the generation of the 2D lookup table for

Table 1 Parameters of the plant, the strip, and the numerical discretization of the constitutive law

Parameter	Symbol	Value
Plant		
Radius bottom roll	r_{BR}	0.8 m
Radius correction and stabilization roll	r_{CR}, r_{SR}	0.125 m
Distance BR–CR	$x_{\mathrm{CR}} - x_{\mathrm{BR}}$	0.42 m
Distance CR–SR	$x_{\mathrm{SR}} - x_{\mathrm{CR}}$	0.395 m
Distance SR–TR	$x_{\mathrm{TR}} - x_{\mathrm{SR}}$	56.8 m
Strip		
Width	b	1 m
Thickness	h	1 mm
Young's modulus	E	160 GPa
Yield stress	σ_{yld}	150 MPa
Constitutive law		
Grid size thickness	Δz	0.042 mm
Grid size curvature	$\Delta \kappa_x$	0.016 m^{-1}

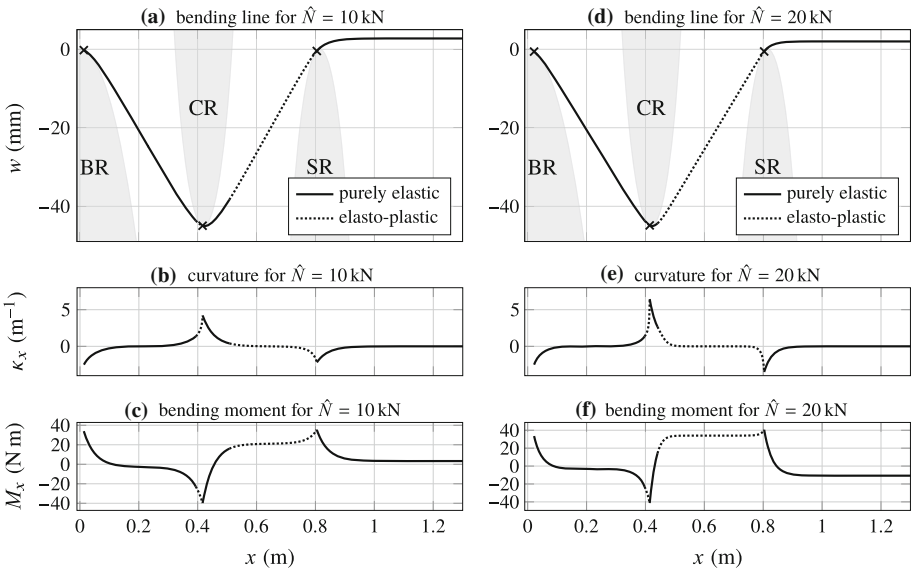

Fig. 7 Bending lines, curvatures, and bending moments for different tensional forces and $z_{\mathrm{CR}} = 45\,\mathrm{mm}$.

the constitutive law takes up to 4 min. If the asymmetric case for a nonvanishing mean strain $\hat{\varepsilon}_{xx}$ is considered. However, if the mean tension is neglected, the lookup table is computed within 8 s. In the presented example, the asymmetric case was simulated. The domain between bottom roll and stabilization roll has been discretized with 167 finite elements, cf. Sect. 4.3. The bending line including the contact points is typically computed within 2–8 s, depending on how much of the strip is plasticized. For the considered load cases with $z_{\mathrm{CR}} \leq 60\,\mathrm{mm}$, the absolute strip slope $|w'| \leq 0.17\,\mathrm{mm}^{-1}$. The absolute values of the contact angles $|\alpha_\rho^c| < 0.16\,\mathrm{rad}$, which would lead to longitudinal components of radial reaction forces at the rolls that are smaller than 2.5% of the tensional force $\hat{N}$. These results show that the assumption of small angles is sufficiently met.

In Fig. 7, the bending lines $w(x)$, the curvatures $\kappa_x(x)$, and the bending moments $M_x(x)$ are shown for an adjustment of the correction roll $z_{\mathrm{CR}} = 45\,\mathrm{mm}$, and two tensional forces $\hat{N} = 10\,\mathrm{kN}$ and $\hat{N} = 20\,\mathrm{kN}$. In both cases, the strip is elasto-plastically bent before it touches the correction and the stabilization roll (dotted sections). The contact points are marked by crosses. In the purely elastic sections, the curvatures in Fig. 7b, e show an exponential evolution according to the analytical solution in (23). In the elasto-plastic sections, just before the contact points, the curvatures undergo a rapid change. In the case of $\hat{N} = 20\,\mathrm{kN}$, cf. Fig. 7e, the extreme curvatures at the correction roll and the stabilization roll are significantly higher than for $\hat{N} = 10\,\mathrm{kN}$, cf. Fig. 7b. The associated bending moments do not vary that much between the two cases because of the saturation characteristic of the bending moment as a function of the curvature.

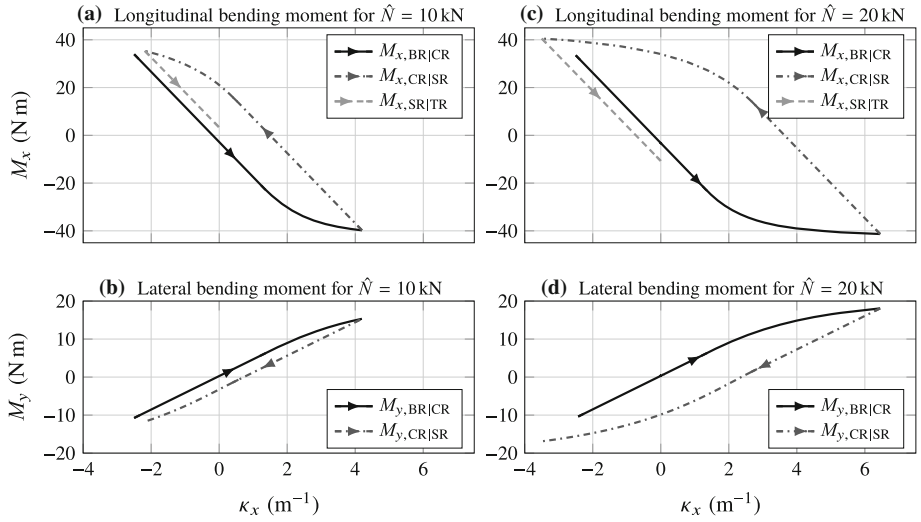

Fig. 8 Bending moment versus curvature

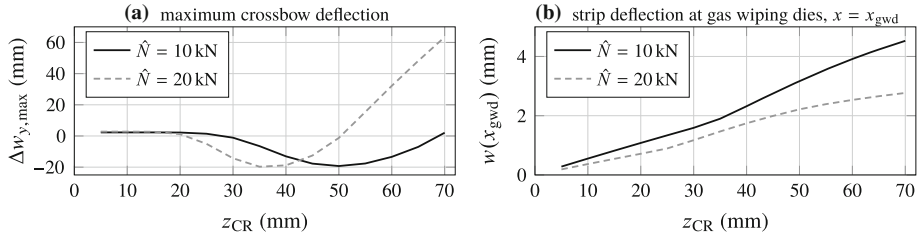

Fig. 9 Maximum crossbow deflection (**a**) and strip deflection at the gas wiping dies (**b**) as functions of the adjustment of the correction roll

These relations between the curvature κ_x and the longitudinal bending moment M_x as well as the lateral bending moment M_y are shown in Fig. 8 for both tensional forces. A comparison of M_x in Fig. 8a, c shows that the magnitude of the curvature $\kappa_{x,\mathrm{SR}}$ at the stabilization roll is considerably higher in the second case. This leads to the observation that, compared to the first case, the bending moment $M_{x,\mathrm{SR|TR}}$ changes its sign for vanishing κ_x, cf. also Fig. 7c, f. In Fig. 8b, d, the lateral bending moment M_y is not given for the domain SR–TR because in this domain the constitutive relation $M_y(\kappa_x)$ based on the assumption $\kappa_y = 0$ is not intended to model the situation where κ_y is generally not restricted. However, the values of the curvature and the lateral bending moment M_y, see Fig. 8b, d, at the stabilization roll are of interest because they define the maximum crossbow deflection $\Delta w_{y,\max}$ of the strip, cf. (37) and (38).

The maximum deflection is shown in Fig. 9a as a function of the adjustment of the correction roll $z_{\mathrm{CR}} \in [5, 70\,\mathrm{mm}]$. Typically, this relation has two zero crossings, cf. [5,8]. The first occurs when only the bending at the correction roll is plastic; the second occurs when also the bending at the correction roll is plastic. The latter case is usually associated with higher contact forces at the rolls. From Fig. 9a, it can be inferred that with higher tensional forces smaller adjustments of the correction roll are required to obtain a vanishing crossbow deflection ($\Delta w_{y,\max} = 0$).

For the considered strip, the deflection at the gas wiping dies (here $x_{\mathrm{gwd}} = 1.2\,\mathrm{m}$, cf. Fig. 2) versus the adjustment of the correction roll is presented in Fig. 9b. The strip is straightened more for higher tensional forces and the deflection at the gas wiping dies is thus smaller. The slight kinks of the curves at $z_{\mathrm{CR}} = 35\,\mathrm{mm}$ ($\hat{N} = 10\,\mathrm{kN}$) and $z_{\mathrm{CR}} = 25\,\mathrm{mm}$ ($\hat{N} = 20\,\mathrm{kN}$) mark the onset of plastic bending at the correction roll.

5.2 Validation

A measurement-based validation of the presented strip model is difficult because the strip deflection cannot be easily measured at the position of the gas wiping dies. However, the operator-defined mean transversal

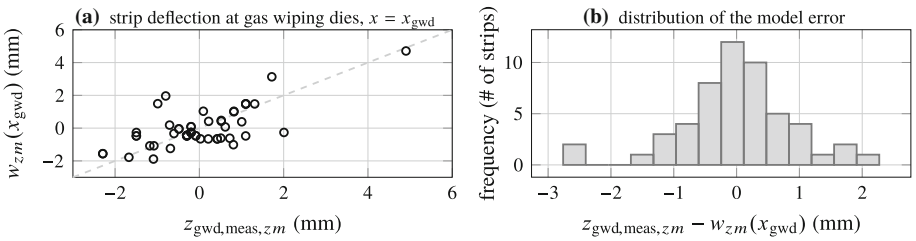

Fig. 10 Comparison of measured and calculated strip deflection at the gas wiping dies for 53 strips from a typical production schedule

adjustment $z_{gwd,meas}$ of the gas wiping dies can be taken as an indicator of the strip deflection that is required to achieve a symmetric zinc coating on both sides of the strip. For a sample of 53 strips from a typical production schedule, this adjustment was compared with the calculated strip deflection $w(x_{gwd})$. Because the absolute value of $z_{gwd,meas}$ is not exactly known, the zero-mean values $z_{gwd,meas,zm} = z_{gwd,meas} - \bar{z}_{gwd,meas}$ and $w_{zm}(x_{gwd}) = w(x_{gwd}) - \bar{w}(x_{gwd})$ are considered, where $\bar{z}_{gwd,meas}$ and $\bar{w}(x_{gwd})$ are the mean values of the respective 53 samples. Figure 10a shows that the model is in good accordance with the approximate measurement for a wide range of deflections. The frequency distribution of the model error affirms this finding. Note that in the model only nominal values of the material parameters E and σ_{yld} were used, the deformation history in the furnace was neglected, and the position of the gas wiping dies might not be exactly aligned with the passline of the strip.

6 Conclusions

A mathematical model that calculates the elasto-plastic deformation of steel strips at the rolls in the zinc bath of a hot-dip galvanizing line is proposed. The computation of the model is efficient because the numerical evaluation of complex elasto-plastic material models and the solution of the boundary value problem of strip bending are separated. The model directly yields the mean strip deflection after the stabilization roll and, based on the elasto-plastic state of deformation at the stabilization roll, the maximum crossbow deflection. These results can be utilized in feedforward control for the position of the gas wiping dies and the correction roll in order to achieve a homogeneous zinc coating that is equal and uniform on both sides of the strip.

Acknowledgements Open access funding provided by TU Wien (TUW). Financial support by the Austrian Federal Ministry of Science, Research and Economy, the National Foundation for Research, Technology and Development, and voestalpine Stahl GmbH is gratefully acknowledged. The second author gratefully acknowledges financial support provided by the Austrian Academy of Sciences in the form of an APART fellowship at the Automation and Control Institute of Vienna University of Technology.

References

1. Baumgart, M., Steinboeck, A., Saxinger, M., Kugi, A.: Elasto-plastic bending of steel strip in a hot-dip galvanizing line. In: Proceedings of the 3rd Polish Congress of Mechanics (PCM) and 21st International Conference on Computer Methods in Mechanics (CMM), Gdansk, Poland, pp. 55–56 (2015)
2. Gerstmayr, J.: Modeling and simulation of elastoplastic multibody systems with damage. Mech. Based Des. Struct. Mach. **31**(2), 201–227 (2003)
3. Gross, D., Hauger, W., Schröder, J., Wall, W.A.: Technische Mechanik, vol. 2, Elastostatik, 9th edn. Springer, Berlin (2007)
4. Hill, R.: The Mathematical Theory of Plasticity. Oxford University Press, Oxford (1950)
5. Hira, T., Abe, H., Azuma, S.: Analysis of sheet metal bending deformation behavior in processing lines and its effectiveness. Kawasaki Steel Tech. Rep. **19**, 54–62 (1988)
6. Huh, H., Lee, H.W., Park, S.R., Kim, G.Y., Nam, S.H.: The parametric process design of tension levelling with an elasto-plastic finite element method. J. Mater. Process. Technol. **113**(1–3), 714–719 (2001)
7. Jung, W., Jang, Y., Lim, S., Won, S.: Active vibration and flatness control of a strip in a continuous galvanizing line using positive position feedback control. ISIJ Int. **53**(5), 854–865 (2013)
8. Masui, T., Kaseda, Y., Ando, K.: Warp control in strip processing plant. ISIJ Int. **31**(3), 262–267 (1991)

9. Misaka, Y., Masui, T.: Shape correction of steel strip by tension leveller. Trans. Iron Steel Inst. Jpn. **18**(8), 475–484 (1978)
10. Pawelski, H., Pawelski, O.: Technische Plastomechanik. Stahleisen, Düsseldorf (2000)
11. Reddy, J.: An Introduction to the Finite Element Method, 3rd edn. McGraw-Hill, New York (2006)
12. Reddy, J.: Theory and Analysis of Elastic Plates and Shells, 2nd edn. CRC Press, Boca Raton (2007)
13. Saxinger, M., Steinboeck, A., Baumgart, M., Kerschbaummayr, P., Kugi, A.: Influence of air cooling jets on the steady-state shape of strips in hot dip galvanizing lines. In: Proceedings of 16th the IFAC Symposium on Control, Optimization and Automation in Mining, Mineral and Metal Processing (MMM), Oulu, Finland, pp. 143–148 (2015)
14. Stadler, G., Steinboeck, A., Baumgart, M., Kugi, A.: Modellierung des Umschlingungswinkels eines auf Rollen geführten Metallbandes. at—Automatisierungstechnik **63**(8), 646–655 (2015)
15. Steinboeck, A., Baumgart, M., Stadler, G., Saxinger, M., Kugi, A.: Dynamical models of axially moving rods with tensile and bending stiffness. In: Proceedings of the 8th Vienna Conference on Mathematical Modelling, Vienna, Austria, pp. 614–619 (2015)
16. Steinwender, L., Kainz, A., Krimpelstätter, K., Zeman, K.: An arbitrary Lagrangian–Eulerian (ALE) approach for the modelling of tension levelling processes. In: Proceedings of the XI International Conference on Computational Plasticity. Fundamentals and Applications (COMPLAS XI). International Center for Numerical Methods in Engineering (CIMNE), Barcelona, Spain (2011)
17. Steinwender, L., Kainz, A., Krimpelstätter, K., Zeman, K.: A novel approach for the modeling of tension leveling processes by employing parametric shape functions. In: Proceedings of the 4th International Conference on Modelling and Simulation of Metallurgical Processes in Steelmaking, STEELSIM, METEC InSteelCon 2011. Düsseldorf, Germany (2011)
18. Zienkiewicz, O., Taylor, R.: The Finite Element Method: For Solid and Structural Mechanics, 6th edn. Elsevier, New York (2005)